

Think-to-Talk or Talk-to-Think? When LLMs Come Up with an Answer in Multi-Step Arithmetic Reasoning

Keito Kudo^{1,2}, Yoichi Aoki^{1,2}, Tatsuki Kuribayashi³, Shusaku Sone¹
Masaya Taniguchi², Ana Brassard^{2,1}, Keisuke Sakaguchi^{1,2}, Kentaro Inui^{3,1,2}

¹Tohoku University, ²RIKEN, ³MBZUAI

{keito.kudo.q4, youichi.aoki.p2, sone.shusaku.r8}@dc.tohoku.ac.jp,
{tatsuki.kuribayashi, kentaro.inui}@mbzuai.ac.ae,
keisuke.sakaguchi@tohoku.ac.jp, {masaya.taniguchi, ana.brassard}@riken.jp

Abstract

This study investigates the internal reasoning process of language models during arithmetic multi-step reasoning, motivated by the question of *when* they internally form their answers during reasoning. Particularly, we inspect whether the answer is determined before or after chain-of-thought (CoT) begins to determine whether models follow a post-hoc *Think-to-Talk* mode or a step-by-step *Talk-to-Think* mode of explanation. Through causal probing experiments in controlled arithmetic reasoning tasks, we found systematic internal reasoning patterns across models in our case study; for example, single-step subproblems are solved before CoT begins, and more complicated multi-step calculations are performed during CoT.

1 Introduction

An explanation may be produced in two modes: as a post-hoc explanation to a predetermined conclusion (*Think-to-Talk*) or by process of reaching a conclusion while explaining (*Talk-to-Think*). An analogy applies to large language models (LLMs) using chain-of-thought (CoT; Wu et al., 2023a) reasoning: *is the output a post-hoc explanation, or does it reflect step-by-step solving?*

To answer this question, we focus on multi-step arithmetic reasoning tasks as a case study and apply causal probing to model internals at each layer during each timestep to determine *when* the answer is reached in CoT-style reasoning. In our experiments, we prepared a controlled testbed of symbolic arithmetic reasoning tasks and observed whether trained classifiers, given a set of hidden representations, could accurately predict the values of all variables in the test instance. By comparing accuracies across each timestep, we can observe at which point the model’s internals start being informative to the probes, illustrating the model’s internal reasoning flow.

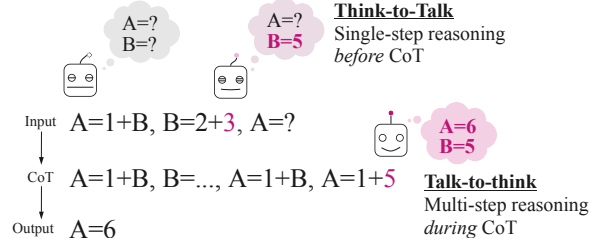


Figure 1: Using linear probes, we investigated at which time during the LLM’s reasoning process it is possible to determine the values of each variable, illustrating the model’s reasoning process.

Our experiments with linear probes reveal intriguing properties of the model’s internal reasoning process. Specifically, not all the reasoning is performed while generating CoT chains (*talk-to-think* mode). Some sub-problems were already resolved immediately after the problem was shown (*think-to-talk* mode). Then, we further found that this *think-to-talk* mode was not randomly adopted; rather, there were systematic tendencies where single-step reasoning (e.g., $A=2+3, A=?$) is performed before CoT, and multi-step reasoning (e.g., $A=2+3, B=A+3, B=?$) follows after CoT (Figure 2).

To enhance the above findings, we conducted causal intervention analyses to inspect whether the pre-resolved sub-answers are referred to in models deriving the final answer. The analyses revealed that such predetermined (sub-)answers indeed impacted the model’s final answer (§ 4.1), but their causal relationship was somewhat indirect (§ 4.2). These reveal a systematic internal reasoning pattern between *Think-to-Talk* and *Talk-to-Think* modes in arithmetic reasoning tasks. This extends existing mechanistic interpretability results of LLMs regarding arithmetic problem solving (Stolfo et al., 2023; Zhu et al., 2025), specifically from simple arithmetic operation to *multi-step* reasoning outputs.¹

¹Code and data are available at <https://github.com/keitokudo/TTT>

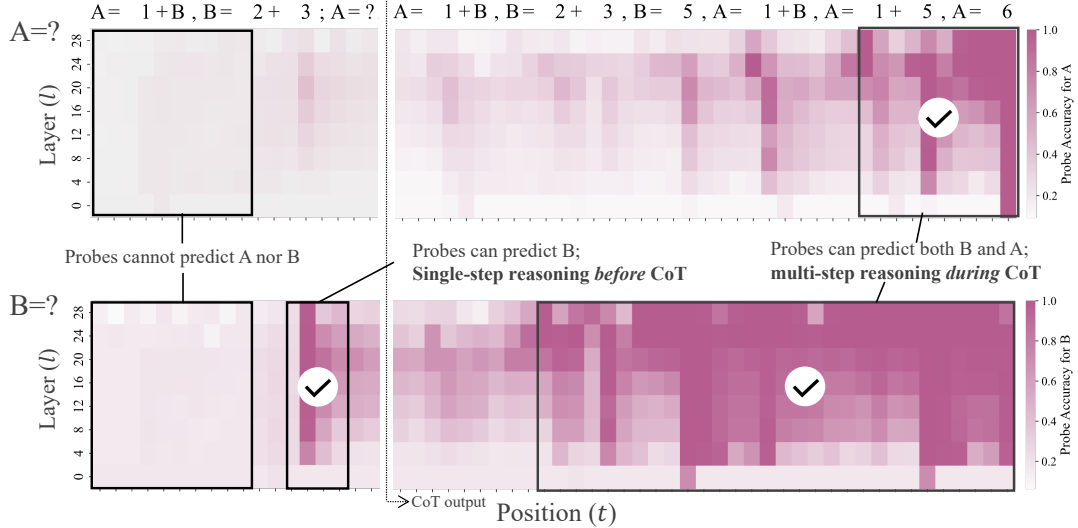


Figure 2: Probes predict each variable’s value from the LMs’ hidden states at each timestep \times layer. The upper heat map shows the probe accuracy for predicting the value of A. The lower one shows the prediction accuracy for the value of B. A high accuracy indicates where the model completes the corresponding calculation (§ 3.3). This result shows the analysis conducted on Qwen2.5-7B for task Level 3.

Level	INPUT	OUTPUT	#Step	#Stack	#Dist.
1	$A = 1 + B_{-3}, B = 2_{-2}; A = ?_{-1}$	$A = 1 + B_0, B = 2_1, A = 1 + B_2, A = 1 + 2_3,$ $A = 3_4$	1	1	0
2	$A = 2 + 3_{-3}, B = 1 + A_{-2}; B = ?_{-1}$	$B = 1 + A_0, A = 2 + 3_1, A = 5_2, B = 1 + A_3,$ $B = 1 + 5_4, B = 6_5$	2	0	0
3	$A = 1 + B_{-3}, B = 2 + 3_{-2}; A = ?_{-1}$	$A = 1 + B_0, B = 2 + 3_1, B = 5_2, A = 1 + B_3,$ $A = 1 + 5_4, A = 6_5$	2	1	0
4	$A = 1 + B_{-4}, B = 2 + 3_{-3}, C = 4 + 5_{-2}; A = ?_{-1}$	$A = 1 + B_0, B = 2 + 3_1, B = 5_2, A = 1 + B_3,$ $A = 1 + 5_4, A = 6_5$	2	1	1
5	$A = 1 + B_{-4}, B = 2 + C_{-3}, C = 1 + 2_{-2}; A = ?_{-1}$	$A = 1 + B_0, B = 2 + C_1, C = 1 + 2_2, C = 3_3,$ $B = 2 + C_4, B = 2 + 3_5, B = 5_6, A = 1 + B_7,$ $A = 1 + 5_8, A = 6_9$	3	2	0

Table 1: Examples of arithmetic reasoning tasks used in our experiments at each complexity level. #Step indicates the number of required operations to reach the final answer. #Stack indicates how many variables’ values are not immediately determined in their first appearing equation. #Dist. is the number of unnecessary distractor equations. The number (e.g., -3) indicated in the lower right corner of each equation represents the equation’s position. This position is used as a reference point for calculating t_{eq}^* in § 3.2.

2 General settings

2.1 Arithmetic problems

We prepared a dataset of multi-step arithmetic problems similarly to Kudo et al. (2023) and Yu (2025). Each sample is a string of assignments (e.g., $A=1$) and operations (e.g., $B=1+3$ or $B=1+A$) ending with a query for a variable’s value (e.g., $B=?$). We also defined five complexity levels, depending on (i) how many equations need to be resolved to reach the answer (#Step in Table 1), (ii) how many variables’ values cannot be immediately resolved (and thus pended to a stack) in their first appearance when incrementally reading the problem from left to right (#Stack), (iii) and the number of unnecessary distractor equations (#Dist.). For example, in

the Level 5 example in Table 1, where #Step is three and #Stack is two, calculating A requires at least three steps of reasoning: $C=(1+2)=3$, $B=(2+3)=5$, and then $A=(1+5)=6$, and two variables need to be resolved before reaching A: B and C.

Notation. Formally, let v denote a variable name sampled from the 26 letters of the English alphabet $\Sigma = \{a, b, c, \dots, z\}$, and d a number sampled from the set of decimal digits $D = \{0, 1, 2, \dots, 9\}$. Each instance consists of multiple equations $[e_1, e_2, \dots, e_n]$ followed by a final query q . Each equation follows the format $v = d$, $v = d \pm d$, or $v = d \pm v$. We denote i -th variable to appear within an instance from the left as v_i . E.g., in the Level 5 example in Table 1, $v_1 = A$, $v_2 = B$,

and $v_3 = C$.² The value assigned to a variable v_i is denoted as $\$\{v_i\} \in D$.

Generation rules. We ensure that $\$\{v_i\}$ for any v_i is also a single-digit number, and $\$\{v_i\}$ is constant within the same instance (i.e., we exclude cases such as $A=1+2, A=B+2, B=6$). All samples of the same complexity level follow the exact same format except for the actual numbers, variable names, and operators, meaning that $\$\{v_i\}$ in each level can be obtained with exactly the same abstract procedure. E.g., first calculate $\$\{v_3\}$, and then calculate $\$\{v_2\}$ with $\$\{v_3\}$, and then finally calculate $\$\{v_1\}$ with $\$\{v_2\}$. Non-duplicated instances are created for each level by varying the variable names, numbers, and operators appearing in the equations. We created 12,000 unique instances in total, of which 10,000 are used for training probing classifiers and 2,000 for testing their accuracy.

2.2 CoT-style inference

Henceforth, we refer to the part before CoT (explained in 2.1) as the INPUT and the CoT-reasoning part as the OUTPUT of an instance. The OUTPUT, as shown in the right part of Table 1, is also a sequence of equations in the same format as the INPUT and can be split into intermediate steps z and a final answer y . For example, for the Level 1 instance in Table 1 (topmost), $x = \text{“}A=1+B, B=2,\text{”}$ $z = \text{“}A=1+B, B=2, A=1+2, A=,\text{”}$ and $y = \text{“}3.\text{”}$ That is, the task is to generate intermediate steps z and derive a final answer y given an INPUT x and a demonstration of three examples. As a sanity check, we confirmed that the target models could follow the expected OUTPUT format and solve the tasks with nearly 100% accuracy in this setting (see appendix A.1 for more details).

We denote a token position within the entire concatenated sequence $x \oplus z \oplus y$ with $t \in \mathbb{Z}$. t is relative to CoT; that is, t is zero where CoT begins, negative within the INPUT, and positive within the OUTPUT. Similarly, we assign an equation position $t_{\text{eq}} \in \mathbb{Z}$ to each equation in the INPUT and OUTPUT (subscripts on the underlines in Table 1).

3 Probing

When do models solve (sub)problems in CoT-style reasoning? Do they (i) finalize reasoning during the INPUT stage, with the CoT as a post-hoc explanation (*Think-to-Talk*), or (ii) solve the task step-by-

²For ease of reading, all examples throughout this paper use the uppercased variables A, B, C, and only the operator +.

step during CoT generation (*Talk-to-Think*)? We address this by examining where the final answer, or the necessary information for it, emerges in the model’s internal representations using linear probes.

3.1 Training settings for linear probes

We train a linear probe (Alain and Bengio, 2017a) for an l -layer LLM ($l = 0$ for the input embedding layer). To identify where the LLM solved a particular (sub)problem, we train a separate probe for each combination of token position $t \in \mathbb{Z}$, layer depth $l \in \mathbb{N}$, and $v_i \in \Sigma$ in each level of the problem. Specifically, given a model’s d -dimensional hidden state $\mathbf{h}_{t,l} \in \mathbb{R}^d$, the probing classifier $f_{t,l,v_i}(\cdot) : \mathbb{R}^d \rightarrow D$ predicts $\$\{v_i\}$. That is, for each (t, l) , we first obtained 10,000 of $\mathbf{h}_{t,l}$ from training instances and then evaluated the accuracy of $f_{t,l,v_i}(\cdot)$ for each v_i with 2,000 hidden states from test instances and the correct $\$\{v_i\}$. If a probe $f_{t,l,v_i}(\cdot)$ achieves high accuracy, this suggests that $\$\{v_i\}$ is already computed at the corresponding position (t and l). Figure 3 illustrates an example of our probing results with a Level 3 task, where, for example, the value of B can be extracted within INPUT and thus already computed before CoT begins.

The probe $f_{t,l,v_i}(\cdot)$ is a single linear transformation; that is, the probe is applied to $\mathbf{h}_{t,l}$ as follows:

$$\begin{aligned} \hat{\$\{v_i\}}_{t,l} &= f_{t,l,v_i}(\mathbf{h}_{t,l}) \\ &= \arg \max_D \mathbf{W}_{t,l,v_i} \mathbf{h}_{t,l} + \mathbf{b}_{t,l,v_i} \end{aligned} \quad (1)$$

where, $\mathbf{W}_{t,l,v_i} \in \mathbb{R}^{|D| \times d}$ and $\mathbf{b}_{t,l,v_i} \in \mathbb{R}^{|D|}$ are the weight and bias parameters of the probe, respectively. The symbol $\hat{\cdot}$ is used to refer to the model’s estimate. We train the probes using stochastic gradient descent (Robbins, 1951) to minimize the cross entropy loss. The hyperparameters are listed in Table 9 in the appendix.

3.2 Evaluation metrics

The probing results from all the token positions t and layers l are aggregated as follows:

$$t^*(v_i) = \min\{t \mid \max_l \text{acc}(t, l, v_i) > \tau\} \quad (2)$$

where $\text{acc}(t, l, v_i) \in [0, 1]$ indicates the accuracy of a probing classifier f_{t,l,v_i} . The $t^*(v_i) \in \mathbb{Z}$ indicates when was the first time the probing classifier achieved a reasonable accuracy above τ ($= 0.90$ in our study³) for the variable v_i . As a more

³See Appendix A.4 for results at different thresholds.

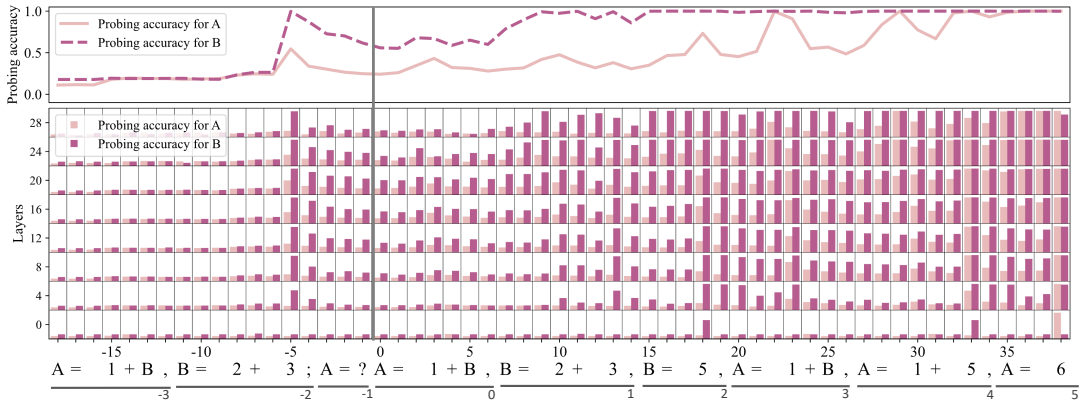


Figure 3: Probing results for Qwen2.5-7B at the task Level 3. The bar graphs in the lower section represent the accuracy of probes computed on the evaluation set. The input sequence below the graphs is just an example; in the actual evaluation set, each variable name, number, and operator are randomly sampled from $(D, \Sigma, \{+, -\})$. The upper part indicates the maximum probing accuracy achieved at each token position t . The bottom part shows the probing accuracies in each token t , layer l , and variable v_i .

coarse but comprehensive value, we also report $t_{\text{eq}}^*(v_i)$ indicating which equation t_{eq} the $t^*(v_i)$ falls into. Given that the t (and t_{eq}) is relative to the CoT-beginning position, if $t_{\text{eq}}^*(v_i)$ is negative, the value $\{v_i\}$ is computed before CoT begins. This is the case for $t^*(i.e., B)$ in Figure 3, based on the spike around $t_{\text{eq}} = -2$ in the upper line graph.

We also report two types of accuracy:

$$\text{Acc}_{<\text{CoT}}(v_i) = \max_{t < 0, l} \text{acc}(t, l, v_i), \quad (3)$$

$$\text{Acc}_{>\text{CoT}}(v_i) = \max_{t \geq 0, l} \text{acc}(t, l, v_i). \quad (4)$$

If $\text{Acc}_{<\text{CoT}}(v_i)$ is sufficiently high, $\{v_i\}$ is resolved internally before CoT begins (*Think-to-Talk* mode). Conversely, if $\text{Acc}_{<\text{CoT}}(v_i)$ is low and $\text{Acc}_{>\text{CoT}}(v_i)$ is high, the answer is derived while performing CoT reasoning (*Talk-to-Think* mode).

3.3 Experimental results

Across task complexity levels. We first analyze Qwen2.5-7B (Qwen Team, 2024) across the five task levels. Table 2 shows t_{eq}^* for each variable as well as the lower bounds of t_{eq}^\dagger , which can be computed with a greedy resolver of equations. The t_{eq}^* scores the same as t_{eq}^\dagger are bolded, and there is an intriguing parallel with the required reasoning steps for each variable, i.e., how many other variables should be referred to compute the respective value (#Step). That is, variables with fewer required reasoning steps ($\#\text{Steps} \leq 1$) achieved the lower bound t_{eq}^\dagger , and vice versa. This clear pattern is also reflected in the contrast between $\text{Acc}_{<\text{CoT}}$

Level	Variable		When (\downarrow)		Acc. (\uparrow)	
	variable	#Step	t_{eq}^*	t_{eq}^\dagger	< CoT	> CoT
1	v_1 (A)	1	-2	-2	99.6	100
	v_2 (B)	0	-2	-2	100	100
2	v_1 (A)	1	-3	-3	100	100
	v_2 (B)	2	3	-2	52.1	100
3	v_1 (A)	2	3	-2	54.7	100
	v_2 (B)	1	-2	-2	99.7	100
4	v_1 (A)	2	4	-3	46.0	100
	v_2 (B)	1	-3	-3	99.2	100
	v_3 (C)	1	-2	-2	99.1	34.5
5	v_1 (A)	3	7	-2	25.1	100
	v_2 (B)	2	5	-2	49.0	100
	v_3 (C)	1	-2	-2	99.8	100

Table 2: The results of Qwen2.5-7B on the five levels. The t_{eq}^* is the time when the model comes up with the correct answer (see § 3.2). The t_{eq}^\dagger column indicates the lower bound of t_{eq}^* score. The $< \text{CoT}$ and $> \text{CoT}$ scores correspond to the accuracies introduced in § 3.2.

and $\text{Acc}_{>\text{CoT}}$ —a larger contrast is shown in variables with many required steps. Furthermore, these patterns have emerged robustly across five levels. The comparison between Levels 2 and 3 perhaps clarifies this pattern the most effectively; these problems only differ in the presentation order of equations (and respective order of variables) and the flipping results for v_1 and v_2 are clearly observed. In summary, the model had selectively solved single-step subproblems before CoT began and resolved multi-step calculations during CoT.

Model	Variable	When (\downarrow)		Acc (\uparrow)	
		t_{eq}^*	t^*	\prec CoT	\succ CoT
Qwen2.5 (7B) (Qwen Team, 2024)	v_1 (A)	3	22	54.7	100
	v_2 (B)	-2	-5	99.7	100
Qwen2.5 (14B) (Qwen Team, 2024)	v_1 (A)	3	22	72.5	100
	v_2 (B)	-2	-5	100	100
Qwen2.5 (32B) (Qwen Team, 2024)	v_1 (A)	3	21	69.7	100
	v_2 (B)	-2	-5	100	100
Qwen2.5-Math (7B) (Yang et al., 2024a)	v_1 (A)	3	22	63.4	100
	v_2 (B)	-2	-5	100	100
Yi1.5 (9B) (Young et al., 2024)	v_1 (A)	4	32	50.0	100
	v_2 (B)	-2	-5	96.5	100
Yi1.5 (34B) (Young et al., 2024)	v_1 (A)	3	25	57.7	100
	v_2 (B)	-2	-5	100	100
Llama3.1 (8B) (Dubey et al., 2024)	v_1 (A)	3	22	63.4	100
	v_2 (B)	-2	-5	92.2	100
Llama3.2 (3B) (Dubey et al., 2024)	v_1 (A)	5	36	47.9	98.0
	v_2 (B)	2	10	86.5	99.5
Mistral-Nemo (12B) (Mistral AI Team, 2024)	v_1 (A)	5	35	39.6	100
	v_2 (B)	-2	-5	91.4	100

Table 3: Results for various models on the task Level 3. The t^* column shows the token-wise time (described in § 3.2), and the other columns are the same as Table 2. The t^* and t_{eq}^* scores that are the same as their lower bounds are bolded.

Across models. We further analyzed ten models listed in Table 3 on the Level 3 task. Almost the same results as Qwen2.5-7B are generally obtained across various models, enhancing the generality of our obtained findings. The $t_{\text{eq}}^*(B)$ score is positive for Llama3.2-3B, but $\text{Acc}_{\prec\text{CoT}}(A)$ is reasonably high (86.5) compared to the variable A, which renders a generally similar trend to the other models (see Figure 21 in Appendix A.5 for detailed results of Llama3.2). For more precise comparisons, the t^* scores tend to be smaller for the larger models, e.g., Yi1.5-34B vs. Yi1.5-9B for variable A. This suggests that larger LLMs can induce the intermediate answer slightly earlier than smaller ones.

3.4 Analysis

Distractors. In task Level 4 (see Table 1), v_3 (C) is a distractor, that is, $\{v_3\}$ is not necessary to derive the final answer. The models can infer this fact from the in-context examples. In contrast, according to Table 2, the $\text{Acc}_{\prec\text{CoT}}(v_3)$ in Level 4 was nearly 100%, while $\text{Acc}_{\succ\text{CoT}}(v_3)$ was relatively low. This indicates that the models try to perform a *brute force* approach, with redundant calculations for all the variables first and then ignoring unnecessary (sub)results.

Setting	Variable	#Step	When (\downarrow)		Acc (\uparrow)	
			t_{eq}^*	t_{eq}^\dagger	\prec CoT	\succ CoT
Same level	v_1	2	4	-3	46.0	100
	v_2	1	-3	-3	99.2	100
	v_3	1	-2	-2	99.1	34.5
General	v_1	2	4	-3	45.8	99.9
	v_2	1	-3	-3	99.9	100
	v_3	1	-2	-2	99.8	45.6

Table 4: Evaluation results of same level prompting and general prompting. Each column is the same as Table 2.

Prompt differences. We investigated whether the format of few-shot prompting influences the model’s internal reasoning patterns. We analyzed the differences between two scenarios: 1. *Same level prompting* and 2. *General prompting*. In the same level prompting scenario, we provided three equations that matched the level of the evaluation task, similar to the general setup (§ 2). Conversely, in the general prompting scenario, the model received 50 randomly generated samples, each containing three equations.⁴ Table 4 compares t_{eq}^* values for these two prompting methods. The experimental results revealed no difference in t_{eq}^* between the two methods. Consequently, the influence of the few-shot prompting format on the model’s internal reasoning patterns appears to be minimal.

Behavior in incorrect instances. Figure 4 shows the top-1 predictions of the probe for B in instances where Llama3.2-3B produced *incorrect* answers for Task 3 (where B happened to be 5). The underlying reason for this remains unclear, but through our probing framework, one can track how such an incorrect answer is propagated to the subsequent generation, which might be practically helpful in debugging the model internals.

4 Causal interventions

In our probing experiments in § 3, we tentatively concluded that simple subproblems are already resolved before CoT begins. However, the exact information flow on how this predetermined answer propagates and eventually affects the final output is unclear. Thus, we perform a causal intervention analysis to investigate the causal dependencies between the predetermined answers identified by our probing (§ 3) and the models’ final answer.

⁴The number of demonstrations in general prompts was larger due to the model’s insufficient performance on the task.

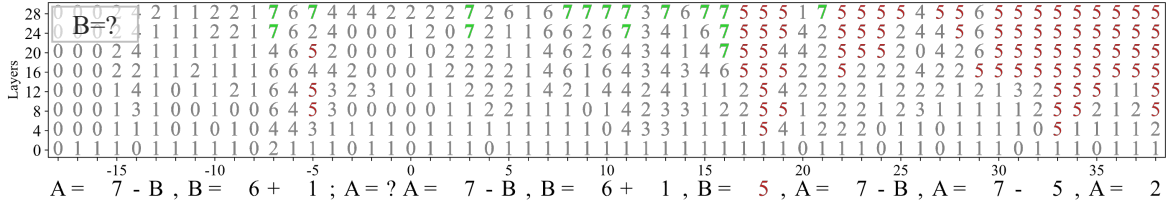


Figure 4: Error analysis of cases where Llama3.2-3B generated *incorrect* answers. The vertical axis represents the index of the transformer layer. The horizontal axis represents the tokens input to the model over time. The numbers in the figure indicate the labels predicted by each probe (top-1) at each layer and time step. The numbers highlighted in green represent the gold labels for the predictions, while those highlighted in red denote the values incorrectly generated by the model.

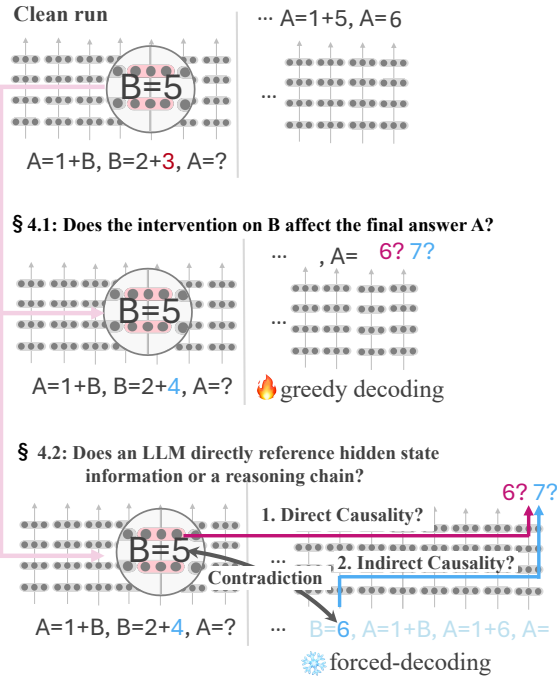


Figure 5: Overview of the causal intervention analysis in § 4 with a specific focus on the relationship between specific hidden states and the model’s final answer.

Activation patching. We employ activation patching (Vig et al., 2020; Meng et al., 2022; Zhang and Nanda, 2024), which is a widely adopted technique for causal intervention analysis in mechanistic interpretability research. Simply put, to inspect the causal relationship between specific hidden states $\mathbf{h}_{t,l}$ and a final answer \hat{y} , we compare two generation scenarios: (i) the ordinary inference and (ii) the intervened inference. In the latter scenario, we replace the specific hidden states $\mathbf{h}_{t,l}$ with other variants $\tilde{\mathbf{h}}_{t,l}$ obtained from the same model but with a different input \tilde{x} (Clean run in Figure 5). The input x and \tilde{x} have different correct answer y and \tilde{y} as well as different chains z and \tilde{z} , respectively. For example, for ($x = \text{“A=1+B, B=2+4; A=?,”}$

$y = 7$), one may use ($\tilde{x} = \text{“A=1+B, B=2+3; A=?,”}$ $\tilde{y} = 6$). If the model’s output turns from y into \tilde{y} due to the intervention to $\mathbf{h}_{t,l}$ with $\tilde{\mathbf{h}}_{t,l}$, we can confirm the causal relationship between $\mathbf{h}_{t,l}$ and the original answer y . We denote the model’s final output without intervention as \hat{y} and that with intervention as $\tilde{\hat{y}}$, respectively (y and \tilde{y} denotes respective gold answers).

Evaluation metrics. We measure the *Success rate* and the *Unchanged rate*. The Success rate indicates how frequently (%) the intervened output $\tilde{\hat{y}}$ aligns with the correct answer \tilde{y} . The Unchanged rate indicates how frequently (%) the intervened output $\tilde{\hat{y}}$ remains the same as y .

4.1 Causality of the probing results

Motivation. In the probing experiments (§ 3), we concluded that a correct answer for a specific variable could be derived from specific hidden states from the INPUT. We reinforce these results by inspecting the causal relationship between hidden states associated with high probing accuracy and the final output, and vice versa.

Patching targets. We specifically focus on Level 3 tasks and Qwen2.5-7B. More specifically, we target the variable v_2 (i.e., B) in the Level 3 format, whose value seems to be pre-resolved internally before CoT begins, based on our probing results. We regard the hidden states $\mathbf{H}^+ = \{\mathbf{h}_{t,l} \mid l \geq 12, -5 \leq t \leq -4\}$ as those associated with high probing accuracy (see Figure 3) and inspect the causal relationship between \mathbf{H}^+ and y (A=6 in the case of Figure 3). In the activation patching, these representations \mathbf{H}^+ are replaced all at once with the intervened representations $\tilde{\mathbf{H}}^+$ (see the next paragraph). We observe the model’s output after the intervention ($\tilde{\hat{y}}$) and aggregate the unchanged rate and success rate

	Target Chain z	Unchanged rate	Success rate
a. H^+	greedy (\tilde{z})	0.00	100
b. H^-	greedy (\tilde{z})	100	0.00
c. H^+	force (z)	100	0.00

Table 5: “Chain” indicates the configuration of reasoning chain output. The “greedy” setting allows the model to generate the reasoning chain by the model itself. The “force” setting refers to the forced decoding of the original chain z that conflicts with the information \tilde{x} injected by the intervention.

across 2,000 test instances. For comparison, we also perform the same intervention experiments using hidden states with low probing accuracies $H^- = \{h_{t,l} \mid l \geq 12, -3 \leq t \leq -1\}$. In this analysis, both H^+ and H^- are from the INPUT; that is, only the INPUT is intervened and fed into the model. The model generates the OUTPUT $\hat{z} \oplus \hat{y}$ with greedy decoding (as explained in § 2).

Counterfactual input and hidden states. As illustrated in Figure 5, we create the counterfactual input \tilde{x} by replacing the last term in the equation of $t_{\text{eq}} = -2$ in the Level 3 format, resulting in different $\{v_1\}$ and $\{v_2\}$. Such input \tilde{x} is fed into the model, and its hidden states of interest, $\tilde{H}^+ = \{\tilde{h}_{t,l} \mid l \geq 12, -5 \leq t \leq -4\}$ and $\tilde{H}^- = \{\tilde{h}_{t,l} \mid l \geq 12, -3 \leq t \leq -1\}$ are saved. Then, those are exploited for the causal intervention analysis.

Results. Table 5 shows the results of the causal intervention. We observed that the intervention to H^+ always altered the final answer y , i.e., $\{A\}$. (a. in Table 5). In contrast, the intervention to H^- never changed the answer (b. in Table 5). This supports the general causal dependencies between the hidden states identified by our probes (§ 3) and the models’ final answer.

4.2 What happens when the predetermined answer conflicts with the reasoning chain?

In § 4.1, our experiments suggested that internally predetermined answers in H^+ affect the final output \hat{y} . However, this observation alone does not reveal the model’s exact internal information flow. Concretely, there remain at least two possible hypotheses on the causal dependencies between H^+ and \hat{y} : (i) *Direct Causality*: the predetermined answer is directly referred to when outputting the final answer ($H^+ \rightarrow \hat{y}$); (ii) *Indirect Causality*: the predetermined answer biases the upcoming reasoning chain z , this effect snowballs through generating

z , and finally biases the answer ($H^+ \rightarrow \hat{z} \rightarrow \hat{y}$). This distinction matters in some practical scenarios as well as scientific questions of LLM internals. For example, in model ensembles or tool-enhanced reasoning, a reasoning chain from another information source can be appended to the model input, which potentially conflicts with its own predetermined answer (or more generally prior knowledge). If the model forms a direct/indirect causality, the model should be insensitive/sensitive to such an alternation to the reasoning chain part. We lastly analyze how strongly the model sticks to its own predetermined answers in such a knowledge conflict scenario (Xu et al., 2024), as a relevant topic to our main experiments.

Setting: To investigate such scenarios, we control the model’s predetermined answer in H^+ as well as reasoning chain z (the bottom part of Figure 5). The setting is the same as § 4.1 except that a particular reasoning chain z is force-decoded. Specifically, H^+ is intervened with \tilde{H}^+ to follow a counterfactual input \tilde{x} ($\dots B=2+3 \dots$), while the chain z follows the non-intervened input x ($\dots B=2+4 \dots$). Now \tilde{x} conflicts with z : $\tilde{x} \oplus z = \text{“}A=1+B, B=2+3, A=?A=1+B, B=2+4 \dots\text{”}$. The question is whether the model outputs y ($A=7$) or \tilde{y} ($A=6$). If the model directly refers to the prior hidden states \tilde{H}^+ in outputting the answer (*Direct causality*), the answer will be \tilde{y} , while if the model refers to the chain z in outputting the answer (*Indirect causality*), the answer will be y . In other words, the dependence between \tilde{H}^+ and z is now blocked ($\tilde{H}^+ \nrightarrow \hat{z} \rightarrow \hat{y}$); the intervention will affect the final answer only in the case of direct causality ($\tilde{H}^+ \rightarrow \hat{y}$). We used the 2,000 instances from Task 3 and Qwen2.5-7B samely as § 4.1.

Results: The generated final answer was *always* consistent with the z ($B=2+4 \dots$) rather than the intervened hidden states \tilde{H}^+ ($B=2+3 \dots$) over all the test instances (c. in Table 5). In summary, the model’s internal prior answer indeed biased the final answer (§ 4.1) but can be easily overwritten by new information in the reasoning chain. This means that *indirect causality* is plausible. In other words, the model’s final answer does not directly refer to its own internal prior answers. This can be seen as two-stage reasoning—they first selectively resolve some simple subproblems (*Think-to-Talk*) and then internally combine, refine, and even discard them during a CoT process (*Talk-to-Think*).

5 Related Work

Analyzing multi-step reasoning in models. Interpreting internal mechanisms of LMs is an active field of study (Conneau et al., 2018; Tenney et al., 2019; Niven and Kao, 2019; nostalgebraist, 2020; Geva et al., 2023; Lieberum et al., 2024; Ghandeharioun et al., 2024; Ferrando and Voita, 2024). Several studies have focused on understanding the mechanisms of multi-step reasoning in particular, both with CoT (Wu et al., 2023a) and other formats. For example, specialized attention heads have been identified for reasoning subtasks such as iterative operations (Cabannes et al., 2024) or decision-making, copying, and induction (Dutta et al., 2024). Dutta et al. (2024) also demonstrated that models gather information from both generated and given context, earlier layers use knowledge learned during pretraining while deeper layers handle context, and models use multiple internal pathways to achieve the final answer. Yang et al. (2024c) showed that, during a two-step latent multi-step reasoning task, language models internally recall *bridge entities*—the connecting concepts used in intermediate reasoning steps. Yang et al. (2024d) further demonstrated that the implicit reasoning ability of the LLMs varied with the type of bridge entity, such as those related to countries being linked to high reasoning capacity and those related to years to low capacity. Furthermore, they noted that multi-step reasoning followed the ability to handle single-step reasoning during pretraining. Focusing on multi-step arithmetic reasoning in particular, Matsumoto et al. (2022) also found evidence of step-by-step calculation in hidden states. However, Yu (2025) found it challenging to detect intermediate results in models not explicitly trained on arithmetic reasoning, implying that the calculations may not occur internally in implicit reasoning. Our work continues in this direction by clarifying where and when models store intermediate results during multi-step calculation.

Internal calculations and numerical representations. How models handle numerical information has also been closely studied. For instance, Heinzlerling and Inui (2024) used partial least squares regression (Wold et al., 2001) to demonstrate that numeric attributes, such as birth years and population numbers, are encoded as monotonic representations in the activation space of LLMs and can be manipulated with interventions. In turn, Stolfo et al. (2023) showed that, in autoregressive LMs,

the operations and numerical information necessary for solving quantitative reasoning are processed in the lower layers of the model, and these results are used by the attention layers to predict the final calculation outcomes. Zhu et al. (2025) studied the representation of numbers in language models’ hidden states during single-hop arithmetic tasks (e.g., What is the sum of 12 and 34?). Their analysis revealed that numerical information is encoded linearly within the hidden states and demonstrated that individual digits could be manipulated independently. In this study, we add to this literature by introducing a *temporal* dimension of analysis, i.e., what numerical information is contained at every time-step of multi-step calculation.

Analysis methods of model internals. Probing (Alain and Bengio, 2017b) is one of the representative methods for analyzing the internal representations of neural models—a small model predicts a specific feature from them, thereby determining whether the input contains information about that feature. In this study, we use them to derive intermediate answers. The causality of this relationship can be further verified by examining if a model’s predictions change when the hidden states are intervened (Li et al., 2023; Wu et al., 2023b). One prominent intervention method is activation patching (Vig et al., 2020; Meng et al., 2022; Zhang and Nanda, 2024), where hidden states obtained from one model instance are transplanted onto another during inference to change its predictions. Such techniques can be applied as a way to control model behavior in practical scenarios such as mitigating inherent biases (Zhao et al., 2019; Ganguli et al., 2023; Yang et al., 2024b). Here, we employ activation patching to validate the plausibility of the probing results.

6 Conclusions

We conducted causal probing analyses of when (sub-)answers are determined in the CoT process, using synthetic arithmetic problems as a controlled testbed. We found systematic evidence of internal reasoning patterns—simple subproblems are solved before the CoT begins, and more complicated multi-step calculations are performed during CoT. Our results extend our understanding of LLMs’ symbolic reasoning process during multi-step reasoning, providing evidence for both a post-hoc *Think-to-Talk* mode and step-by-step *Talk-to-Think* mode of explanation.

Limitations

Comprehensiveness of experimental settings

Some experiments were conducted with a limited scope; for example, the experiments with various models in § 3.3 are conducted only on the Level 3 task. Additionally, causal interventions (§ 4) are performed only with Qwen2.5-7B. Conducting our experiment with more models and tasks will further enhance the generalizability of the results.

Variety of task We analyzed the internal reasoning patterns of language models using synthetic arithmetic reasoning tasks. The use of synthetic data allows for more detailed control compared to experiments on natural language tasks. However, vocabulary and expression diversity, for example, are limited compared to natural language tasks. Therefore, conducting similar analyses on reasoning tasks will verify whether the results of this study apply to other broader, realistic contexts as well.

Probing methods Interpreting internal mechanisms of LMs using probing have been actively conducted in our field (Conneau et al., 2018; Tenney et al., 2019; Campbell et al., 2023; Li et al., 2023); however, there are criticisms regarding the validity of some probing approaches (Liu et al., 2023; Burns et al., 2023). One way to overcome such concerns will be to analyze the generality of obtained results through more diverse methodologies (Gurnee et al., 2023; Bricken et al., 2023).

Ethics statement

This paper will not raise particular ethical concerns, considering that (i) no human experiments were conducted, and (ii) our tasks do not involve ethically sensitive topics.

References

- Guillaume Alain and Yoshua Bengio. 2017a. [Discovering latent knowledge in language models without supervision](#). In *5th International Conference on Learning Representations, ICLR 2017, Toulon, France, April 24-26, 2017, Workshop Track Proceedings*. OpenReview.net.
- Guillaume Alain and Yoshua Bengio. 2017b. [Understanding intermediate layers using linear classifier probes](#). In *5th International Conference on Learning Representations, ICLR 2017, Toulon, France, April 24-26, 2017, Workshop Track Proceedings*. OpenReview.net.
- Trenton Bricken, Adly Templeton, Joshua Batson, Brian Chen, Adam Jermyn, Tom Conerly, Nicholas L. Turner, Cem Anil, Carson Denison, Amanda Askell, Robert Lasenby, Yifan Wu, Shauna Kravec, Nicholas Schiefer, Tim Maxwell, Nicholas Joseph, Alex Tamkin, Karina Nguyen, Brayden McLean, and 5 others. 2023. [Towards monosemanticity: Decomposing language models with dictionary learning](#). In *Anthropic*.
- Collin Burns, Haotian Ye, Dan Klein, and Jacob Steinhardt. 2023. [Discovering latent knowledge in language models without supervision](#). In *The Eleventh International Conference on Learning Representations*.
- Vivien Cabannes, Charles Arnal, Wassim Bouaziz, Xingyu Alice Yang, Francois Charton, and Julia Kempe. 2024. [Iteration head: A mechanistic study of chain-of-thought](#). In *The Thirty-eighth Annual Conference on Neural Information Processing Systems*.
- James Campbell, Phillip Guo, and Richard Ren. 2023. [Localizing lying in Llama: Understanding instructed dishonesty on true-false questions through prompting, probing, and patching](#). In *Socially Responsible Language Modelling Research*.
- Alexis Conneau, German Kruszewski, Guillaume Lample, Loïc Barrault, and Marco Baroni. 2018. [What you can cram into a single \$\\$&!#*\$ vector: Probing sentence embeddings for linguistic properties](#). In *Proceedings of the 56th Annual Meeting of the Association for Computational Linguistics (Volume 1: Long Papers)*, pages 2126–2136, Melbourne, Australia. Association for Computational Linguistics.
- Abhimanyu Dubey, Abhinav Jauhri, Abhinav Pandey, Abhishek Kadian, Ahmad Al-Dahle, Aiesha Letman, Akhil Mathur, Alan Schelten, Amy Yang, Angela Fan, Anirudh Goyal, Anthony Hartshorn, Aobo Yang, Archi Mitra, Archie Sravankumar, Artem Korenev, Arthur Hinsvark, Arun Rao, Aston Zhang, and 82 others. 2024. [The Llama 3 herd of models](#). *CoRR*, abs/2407.21783.
- Subhabrata Dutta, Joykirat Singh, Soumen Chakrabarti, and Tanmoy Chakraborty. 2024. [How to think step-by-step: A mechanistic understanding of chain-of-thought reasoning](#). *Transactions on Machine Learning Research*.
- Javier Ferrando and Elena Voita. 2024. [Information flow routes: Automatically interpreting language models at scale](#). In *Proceedings of the 2024 Conference on Empirical Methods in Natural Language Processing*, pages 17432–17445, Miami, Florida, USA. Association for Computational Linguistics.
- Deep Ganguli, Amanda Askell, Nicholas Schiefer, Thomas I Liao, Kamilè Lukošiūtė, Anna Chen, Anna Goldie, Azalia Mirhoseini, Catherine Olsson, Danny Hernandez, and 1 others. 2023. [The capacity for moral self-correction in large language models](#). *arXiv preprint arXiv:2302.07459*.

- Mor Geva, Jasmijn Bastings, Katja Filippova, and Amir Globerson. 2023. [Dissecting recall of factual associations in auto-regressive language models](#). In *The 2023 Conference on Empirical Methods in Natural Language Processing*.
- Asma Ghandeharioun, Avi Caciularu, Adam Pearce, Lucas Dixon, and Mor Geva. 2024. [Patchscopes: A unifying framework for inspecting hidden representations of language models](#). In *Forty-first International Conference on Machine Learning, ICML 2024, Vienna, Austria, July 21-27, 2024*. OpenReview.net.
- Wes Gurnee, Neel Nanda, Matthew Pauly, Katherine Harvey, Dmitrii Troitskii, and Dimitris Bertsimas. 2023. [Finding neurons in a haystack: Case studies with sparse probing](#). *Transactions on Machine Learning Research*.
- Benjamin Heinzerling and Kentaro Inui. 2024. [Monotonic representation of numeric attributes in language models](#). In *Proceedings of the 62nd Annual Meeting of the Association for Computational Linguistics (Volume 2: Short Papers)*, pages 175–195, Bangkok, Thailand. Association for Computational Linguistics.
- Diederik P. Kingma and Jimmy Ba. 2015. Adam: A Method for Stochastic Optimization. In *3rd International Conference on Learning Representations, ICLR, San Diego, CA, USA, May 7-9, 2015, Conference Track Proceedings*.
- Keito Kudo, Yoichi Aoki, Tatsuki Kuribayashi, Ana Brassard, Masashi Yoshikawa, Keisuke Sakaguchi, and Kentaro Inui. 2023. Do Deep Neural Networks Capture Compositionality in Arithmetic Reasoning? In *Proceedings of the 17th Conference of the European Chapter of the Association for Computational Linguistics (EACL)*, pages 1351–1362.
- Kenneth Li, Aspen K Hopkins, David Bau, Fernanda Viégas, Hanspeter Pfister, and Martin Wattenberg. 2023. Emergent World Representations: Exploring a Sequence Model Trained on a Synthetic Task. In *The Eleventh International Conference on Learning Representations (ICLR)*.
- Tom Lieberum, Senthoran Rajamanoharan, Arthur Conmy, Lewis Smith, Nicolas Sonnerat, Vikrant Varma, János Kramár, Anca D. Dragan, Rohin Shah, and Neel Nanda. 2024. [Gemma scope: Open sparse autoencoders everywhere all at once on Gemma 2](#). *CoRR*, abs/2408.05147.
- Kevin Liu, Stephen Casper, Dylan Hadfield-Menell, and Jacob Andreas. 2023. [Cognitive dissonance: Why do language model outputs disagree with internal representations of truthfulness?](#) In *Proceedings of the 2023 Conference on Empirical Methods in Natural Language Processing*, pages 4791–4797, Singapore. Association for Computational Linguistics.
- Ilya Loshchilov and Frank Hutter. 2017. SGDR: stochastic gradient descent with warm restarts. In *5th International Conference on Learning Representations, ICLR, Toulon, France, April 24-26, 2017, Conference Track Proceedings*.
- Yuta Matsumoto, Benjamin Heinzerling, Masashi Yoshikawa, and Kentaro Inui. 2022. Tracing and Manipulating intermediate values in Neural Math Problem Solvers. In *Proceedings of the 1st Workshop on Mathematical Natural Language Processing (MathNLP)*, pages 1–6.
- Kevin Meng, David Bau, Alex Andonian, and Yonatan Belinkov. 2022. [Locating and editing factual associations in GPT](#). In *Advances in Neural Information Processing Systems*, volume 35, pages 17359–17372. Curran Associates, Inc.
- Mistral AI Team. 2024. [Mistral NeMo](#).
- Timothy Niven and Hung-Yu Kao. 2019. [Probing neural network comprehension of natural language arguments](#). In *Proceedings of the 57th Annual Meeting of the Association for Computational Linguistics*, pages 4658–4664, Florence, Italy. Association for Computational Linguistics.
- nostalgebraist. 2020. [interpreting GPT: the logit lens](#). *LessWrong*.
- Qwen Team. 2024. [Qwen2.5: A party of foundation models](#).
- Herbert E. Robbins. 1951. A stochastic approximation method. *Annals of Mathematical Statistics*, 22:400–407.
- Alessandro Stolfo, Yonatan Belinkov, and Mrinmaya Sachan. 2023. [A mechanistic interpretation of arithmetic reasoning in language models using causal mediation analysis](#). In *Proceedings of the 2023 Conference on Empirical Methods in Natural Language Processing*, pages 7035–7052, Singapore. Association for Computational Linguistics.
- Ian Tenney, Patrick Xia, Berlin Chen, Alex Wang, Adam Poliak, R Thomas McCoy, Najoung Kim, Benjamin Van Durme, Sam Bowman, Dipanjan Das, and Ellie Pavlick. 2019. [What do you learn from context? probing for sentence structure in contextualized word representations](#). In *International Conference on Learning Representations*.
- Ashish Vaswani, Noam Shazeer, Niki Parmar, Jakob Uszkoreit, Llion Jones, Aidan N Gomez, Łukasz Kaiser, and Illia Polosukhin. 2017. Attention Is All You Need. In *Advances in Neural Information Processing Systems 31 (NIPS)*, pages 5998–6008.
- Jesse Vig, Sebastian Gehrmann, Yonatan Belinkov, Sharon Qian, Daniel Nevo, Yaron Singer, and Stuart Shieber. 2020. [Investigating gender bias in language models using causal mediation analysis](#). In *Advances in Neural Information Processing Systems*, volume 33, pages 12388–12401. Curran Associates, Inc.
- Svante Wold, Michael Sjöström, and Lennart Eriksson. 2001. [PLS-regression: a basic tool of chemometrics](#). *Chemometrics and Intelligent Laboratory Systems*, 58(2):109–130. PLS Methods.

- Thomas Wolf, Lysandre Debut, Victor Sanh, Julien Chaumond, Clement Delangue, Anthony Moi, Pierric Cistac, Tim Rault, Rémi Louf, Morgan Funtowicz, Joe Davison, Sam Shleifer, Patrick von Platen, Clara Ma, Yacine Jernite, Julien Plu, Canwen Xu, Teven Le Scao, Sylvain Gugger, and 3 others. 2020. [Transformers: State-of-the-art natural language processing](#). In *Proceedings of the 2020 Conference on Empirical Methods in Natural Language Processing: System Demonstrations*, pages 38–45, Online. Association for Computational Linguistics.
- Dingjun Wu, Jing Zhang, and Xinmei Huang. 2023a. Chain of Thought Prompting Elicits Knowledge Augmentation. In *Findings of the Association for Computational Linguistics (ACL)*, pages 6519–6534.
- Zhengxuan Wu, Atticus Geiger, Thomas Icard, Christopher Potts, and Noah Goodman. 2023b. [Interpretability at scale: Identifying causal mechanisms in alpaca](#). In *Thirty-seventh Conference on Neural Information Processing Systems*.
- Rongwu Xu, Zehan Qi, Zhijiang Guo, Cunxiang Wang, Hongru Wang, Yue Zhang, and Wei Xu. 2024. Knowledge conflicts for llms: A survey. *arXiv preprint arXiv:2403.08319*.
- An Yang, Beichen Zhang, Binyuan Hui, Bofei Gao, Bowen Yu, Chengpeng Li, Dayiheng Liu, Jianhong Tu, Jingren Zhou, Junyang Lin, Keming Lu, Mingfeng Xue, Runji Lin, Tianyu Liu, Xingzhang Ren, and Zhenru Zhang. 2024a. Qwen2.5-math technical report: Toward mathematical expert model via self-improvement. *arXiv preprint arXiv:2409.12122*.
- Nakyeong Yang, Taegwan Kang, Stanley Jungkyu Choi, Honglak Lee, and Kyomin Jung. 2024b. [Mitigating biases for instruction-following language models via bias neurons elimination](#). In *Proceedings of the 62nd Annual Meeting of the Association for Computational Linguistics (Volume 1: Long Papers)*, pages 9061–9073, Bangkok, Thailand. Association for Computational Linguistics.
- Sohee Yang, Elena Gribovskaya, Nora Kassner, Mor Geva, and Sebastian Riedel. 2024c. [Do large language models latently perform multi-hop reasoning?](#) In *Proceedings of the 62nd Annual Meeting of the Association for Computational Linguistics (Volume 1: Long Papers)*, pages 10210–10229, Bangkok, Thailand. Association for Computational Linguistics.
- Sohee Yang, Nora Kassner, Elena Gribovskaya, Sebastian Riedel, and Mor Geva. 2024d. [Do large language models perform latent multi-hop reasoning without exploiting shortcuts?](#) *CoRR*, abs/2411.16679.
- Alex Young, Bei Chen, Chao Li, Chengen Huang, Ge Zhang, Guanwei Zhang, Heng Li, Jiangcheng Zhu, Jianqun Chen, Jing Chang, Kaidong Yu, Peng Liu, Qiang Liu, Shawn Yue, Senbin Yang, Shiming Yang, Tao Yu, Wen Xie, Wenhao Huang, and 11 others. 2024. [Yi: Open foundation models by 01.ai](#). *CoRR*, abs/2403.04652.
- Yijiong Yu. 2025. [Do LLMs really think step-by-step in implicit reasoning?](#) *Preprint*, arXiv:2411.15862.
- Fred Zhang and Neel Nanda. 2024. [Towards best practices of activation patching in language models: Metrics and methods](#). In *The Twelfth International Conference on Learning Representations*.
- Susan Zhang, Stephen Roller, and Naman Goyal et al. 2022. OPT: Open Pre-trained Transformer Language Models. *CoRR*, arXiv preprint, cs.CL/arXiv:2205.01068.
- Jieyu Zhao, Tianlu Wang, Mark Yatskar, Ryan Cotterell, Vicente Ordonez, and Kai-Wei Chang. 2019. [Gender bias in contextualized word embeddings](#). In *Proceedings of the 2019 Conference of the North American Chapter of the Association for Computational Linguistics: Human Language Technologies, Volume 1 (Long and Short Papers)*, pages 629–634, Minneapolis, Minnesota. Association for Computational Linguistics.
- Fangwei Zhu, Damai Dai, and Zhifang Sui. 2025. [Language models encode the value of numbers linearly](#). In *Proceedings of the 31st International Conference on Computational Linguistics*, pages 693–709, Abu Dhabi, UAE. Association for Computational Linguistics.

Model	Level Task	
Qwen2.5 (7B)	1	100
	2	100
	3	100
	4	100
	5	100
Qwen2.5 (14B)	3	100
Qwen2.5 (32B)	3	100
Qwen2.5-Math (7B)	3	100
Yi1.5 (9B)	3	100
Yi1.5 (34B)	3	100
Llama3.1 (8B)	3	100
Llama3.2 (3B)	3	97.6
Mistral-Nemo (12B)	3	99.6

Table 6: The performance of language models on the arithmetic reasoning tasks. The Task column shows the accuracy for the evaluation set (exact match).

A Supplemental results

A.1 Performance of language models in the arithmetic tasks

Table 6 shows the accuracy of language models on arithmetic reasoning tasks for each experimental setting. We computed the accuracy based on exact matches between the output, including the chain ($\hat{z} \oplus \hat{y}$), and the gold labels ($z \oplus y$). The accuracy for all models is nearly 100%, indicating that they are capable of solving the arithmetic reasoning tasks used in this experiment.

A.2 Additional instances of probe predictions for Llama3.2

Figure 8 shows the probe predictions for instances where Llama3.2-3B generates incorrect answers, in addition to the examples shown in Figure 4. In contrast, Figure 9 illustrates the probe predictions for instances where Llama3.2-3B generates correct responses.

A.3 Visualization of activation patching

Figure 7 shows the visualization of the probing results when activation patching is applied in § 4.1. The gray boxes highlight the areas where the hidden states of other problems have been patched. The accuracy of the probes in the patched areas exhibits a significant decline, confirming that the model’s internal state changed.

A.4 Effect of the threshold τ

Table 7 and 8 show the results when the threshold τ is set to 0.85 and 0.95, respectively. The results with different thresholds are still consistent

Model	Variable	When (\downarrow)	
		t_{eq}^*	t^*
Qwen2.5 (7B) (Qwen Team, 2024)	v_1 (A)	3	22
	v_2 (B)	-2	-5
Qwen2.5 (14B) (Qwen Team, 2024)	v_1 (A)	3	22
	v_2 (B)	-2	-5
Qwen2.5 (32B) (Qwen Team, 2024)	v_1 (A)	2	18
	v_2 (B)	-2	-5
Qwen2.5-Math (7B) (Yang et al., 2024a)	v_1 (A)	2	18
	v_2 (B)	-2	-5
Yi1.5 (9B) (Young et al., 2024)	v_1 (A)	3	25
	v_2 (B)	-2	-5
Yi1.5 (34B) (Young et al., 2024)	v_1 (A)	3	25
	v_2 (B)	-2	-5
Llama3.1 (8B) (Dubey et al., 2024)	v_1 (A)	3	22
	v_2 (B)	-2	-5
Llama3.2 (3B) (Dubey et al., 2024)	v_1 (A)	3	22
	v_2 (B)	-2	-5
Mistral-Nemo (12B) (Mistral AI Team, 2024)	v_1 (A)	4	29
	v_2 (B)	-2	-5

Table 7: Results for various models on the task Level 3. In contrast to the results shown in Table 3, the values t_{eq}^* and t^* is computed with $\tau = 0.85$.

with our original observations, which is that most models induced the value of B before CoT:

- When $\tau = 0.85$, $t^*(\text{B})$ is negative for all models (Table 7).
- When $\tau = 0.90$, $t^*(\text{B})$ is positive only for Llama3.2-3B (Table 3).
- When $\tau = 0.95$, $t^*(\text{B})$ is positive for only two models, Llama3.1(8B) and Llama3.2(3B) (Table 8).

A.5 All probing results

Figures 10 to 22 show the probing results for all models and tasks mentioned in this paper.

B Hyperparameters

Table 9 shows the hyperparameters used for training the probes.

C Models trained from scratch

As a sanity check to confirm that our probing approach indeed renders different results depending on the targeted models, we compare the probing results between two models trained on biased synthetic datasets.

Model	Variable	When (\downarrow)	
		t_{eq}^*	t^*
Qwen2.5 (7B) (Qwen Team, 2024)	v_1 (A)	3	22
	v_2 (B)	-2	-5
Qwen2.5 (14B) (Qwen Team, 2024)	v_1 (A)	3	22
	v_2 (B)	-2	-5
Qwen2.5 (32B) (Qwen Team, 2024)	v_1 (A)	3	21
	v_2 (B)	-2	-5
Qwen2.5-Math (7B) (Yang et al., 2024a)	v_1 (A)	3	22
	v_2 (B)	-2	-5
Yi1.5 (9B) (Young et al., 2024)	v_1 (A)	4	32
	v_2 (B)	-2	-5
Yi1.5 (34B) (Young et al., 2024)	v_1 (A)	3	25
	v_2 (B)	-2	-5
Llama3.1 (8B) (Dubey et al., 2024)	v_1 (A)	3	22
	v_2 (B)	1	11
Llama3.2 (3B) (Dubey et al., 2024)	v_1 (A)	5	36
	v_2 (B)	2	16
Mistral-Nemo (12B) (Mistral AI Team, 2024)	v_1 (A)	5	36
	v_2 (B)	1	10

Table 8: Results for various models on the task Level 3. In contrast to the results shown in Table 3, the values t_{eq}^* and t^* is computed with $\tau = 0.85$.

#train instances	10,000
Optimizer	SGD (Robbins, 1951)
Learning rate	1.0×10^{-3} (constant)
Batch size	10,000
Epochs	10,000

Table 9: Hyperparameters for training the probe

C.1 Settings

We used the Level 4 task introduced in Table 1 as an evaluation task. We analyze the two transformer-based LMs:⁵

- **EXPERT model:** This model is trained only on Level 4. That is, the model can know, for example, C (v_3) is unnecessary to calculate the final answer A=? (v_1) and memorize the solution, i.e., add the first three numbers.
- **GENERAL model:** This model is trained on problems consisting of random combinations of three or fewer equations.

The texts are tokenized at the character level. We use the absolute position embeddings from the Transformer (Vaswani et al., 2017) as embeddings for each digit to make it easy for the model to learn

⁵We used Hugging Face Transformers (Wolf et al., 2020) as the implementation.

Architecture	
Base Architecture	OPT (Zhang et al., 2022)
Transformer layers	8
Hidden size	1,024
Feed-forward size	4,096
Attention heads	16
Hyperparameters for Expert model	
#train instances	200,000
Optimizer	Adam (Kingma and Ba, 2015) ($\beta_1 = 0.9, \beta_2 = 0.999, \epsilon = 1 \times 10^{-8}$)
Learning rate scheduler	cosine (Loshchilov and Hutter, 2017)
Learning rate warmup	500
Learning rate (maximum)	3.0×10^{-5}
Gradient clipping	1.0
Dropout	0.1
Batch size	16,384 tokens
Epochs	500
Hyperparameters for General model	
#train instances	1,000,000
Optimizer	Adam (Kingma and Ba, 2015) ($\beta_1 = 0.9, \beta_2 = 0.999, \epsilon = 1 \times 10^{-8}$)
Learning rate scheduler	cosine (Loshchilov and Hutter, 2017)
Learning rate warmup	500
Learning rate (maximum)	1.0×10^{-4}
Gradient clipping	1.0
Dropout	0.1
Batch size	16,384 tokens
Epochs	50

Table 10: Hyperparameters and model architecture for GENERAL and EXPERT model

the magnitude relationships between digits. We use randomly initialized embeddings for variables, operators, and other non-numeric embeddings, and freeze all parameters in embeddings during training. Table 10 shows the hyperparameters and model architecture for the General Model and Expert model.

C.2 Experimental results

Figure 6 and Table 11 show the results of the probing for the GENERAL model and EXPERT model. We confirmed that both models achieved an accuracy of over 99.9% on the test set. The results show strikingly different pictures between the two models. For example, in the EXPERT model, the probe accuracy for B (v_2) never reached nearly 100% (Table 11) probably due to its memorization of shallow solution (i.e., add the first three numbers). In contrast, in the GENERAL model, the probe accuracy for A (v_1) increased, followed by an increase in the probe accuracy for B (v_2) (Figure 6).

Furthermore, only the GENERAL model computes the value of the distractor(C), i.e., the EXPERT model skipped the calculation of the distractor. Furthermore, only the GENERAL model computes the value of the distractor (C); i.e., the EXPERT model

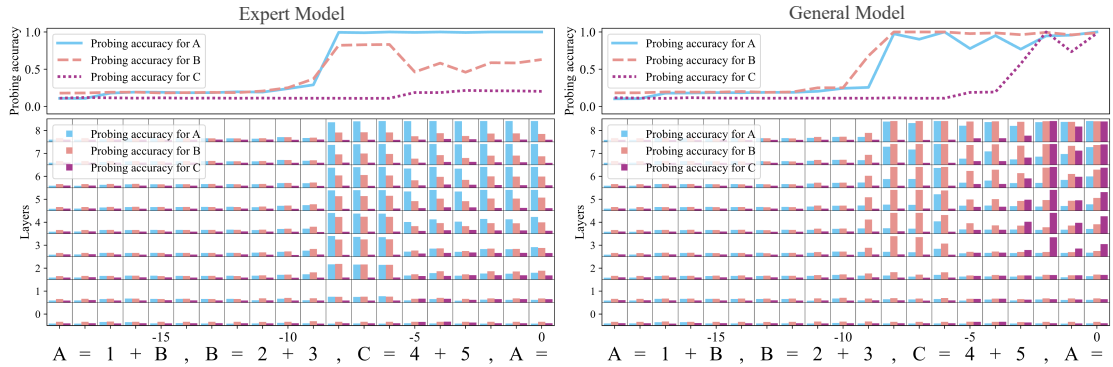


Figure 6: Probing results for models trained only on arithmetic reasoning tasks. The vertical axis represents the index of the transformer layer. The horizontal axis represents the tokens input to the model over time. The vertical axis of the line graph shows the maximum accuracy of the probes at each position (time) t . It can be observed that the probe accuracy for the value of v_3 , an unnecessary equation for the final answer, is low in the EXPERT model.

		When (\downarrow)		Acc (\uparrow)		
		#Step	t_{eq}^*	t^*	Max	Task
Expert model	v_1	2	-2	-8	100.0	
	v_2	1	-	-	83.2	100.0
	v_3	1	-	-	21.5	
General model	v_1	2	-2	-8	100.0	
	v_2	1	-2	-8	98.8	99.9
	v_3	1	-1	-2	98.2	

Table 11: The results of the EXPERT model and GENERAL model. The meanings of all columns except Max are the same as those shown in Table 2. The Max scores refer to the highest accuracy achieved by the probe among all positions. The Task column shows the accuracy for the evaluation set (exact match). “-” indicates that the accuracy of the probes never reached the threshold ($\tau = 0.9$).

skipped the calculation of the distractor. Specifically, the probe accuracy for predicting the value of C reaches a maximum of 98.2% in the GENERAL model, while it is only 21.5% in the EXPERT model. This suggests that the GENERAL model performs calculations for all equations, regardless of the necessity for the final answer. Such different and intuitive results between the two models support the fact that our probing approach can indeed render their different internals for different models.

Moreover, one can also see some consistent patterns between the two models; for example, in both EXPERT and GENERAL models, the probe accuracy for predicting A (v_1) increases immediately after they take necessary information to determine the value of A (v_1). This suggests that the model uses a greedy strategy, executing calculations immediately when the answer is within reach. This ap-

proach is similar to unification in evaluation strategies for programming languages.

D Computational resources

We used NVIDIA A100 GPUs (40GB and 80GB memory) and NVIDIA H100 GPUs to conduct this study.

E Usage of AI assistants

For writing this paper and the source code for the experiments, we use AI assistants (e.g., ChatGPT, GitHub Copilot). However, the use is limited to purposes such as code completion, translation, text editing, and table creation, and all content is solely based on the authors’ ideas.



Figure 7: Probing results when activation patching is applied. The vertical axis represents the index of the transformer layer. The horizontal axis represents the tokens input to the model over time. The name of each setting corresponds to the setting names listed in Table 5. The gray boxes highlight the areas where the hidden states are patched.

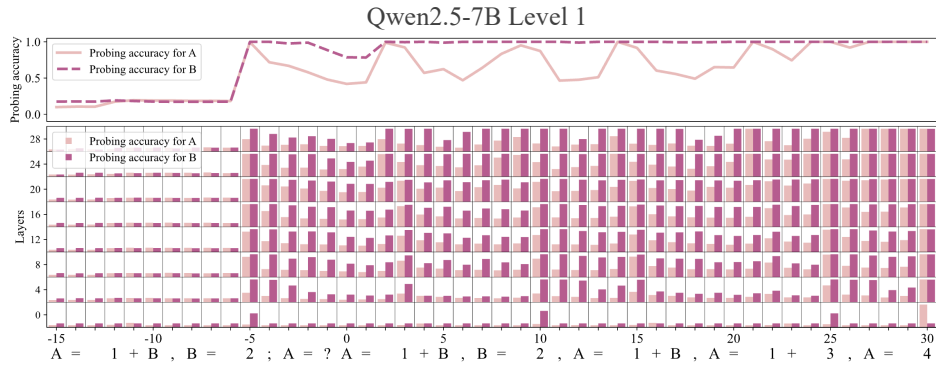


Figure 10: Probing results when Qwen2.5-7B solves Level 1.

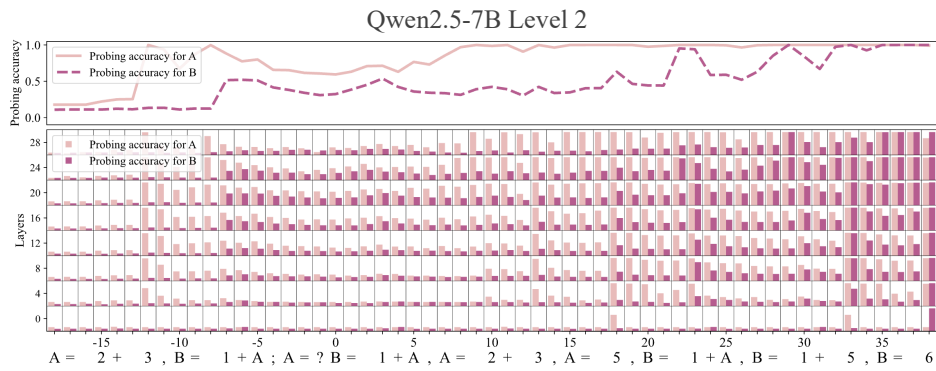


Figure 11: Probing results when Qwen2.5-7B solves Level 2.

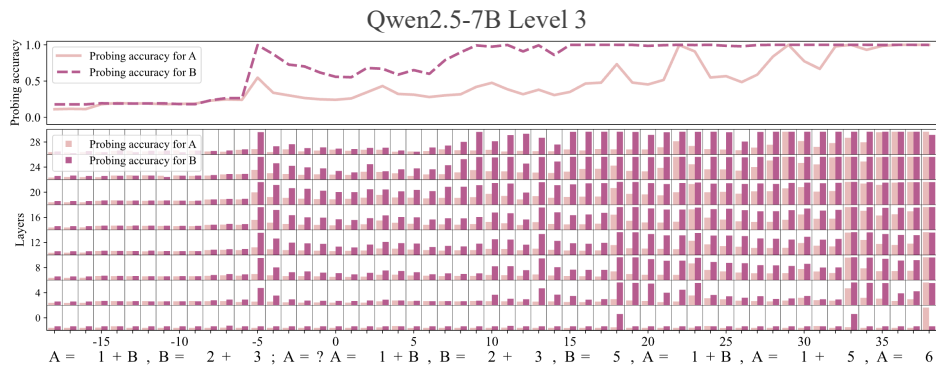


Figure 12: Probing results when Qwen2.5-7B solves Level 3.

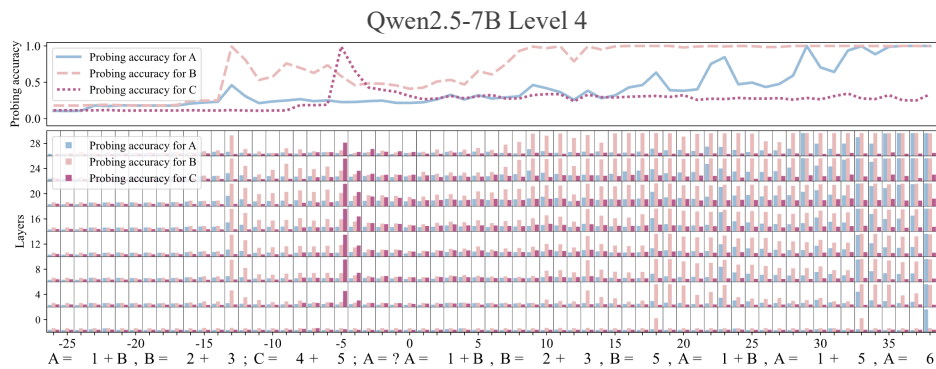


Figure 13: Probing results when Qwen2.5-7B solves Level 4.

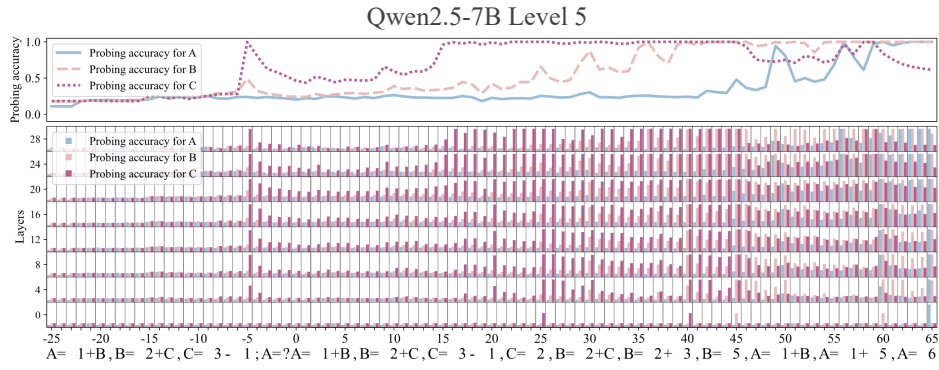


Figure 14: Probing results when Qwen2.5-7B solves Level 5.



Figure 15: Probing results when Qwen2.5-14B solves Level 3.

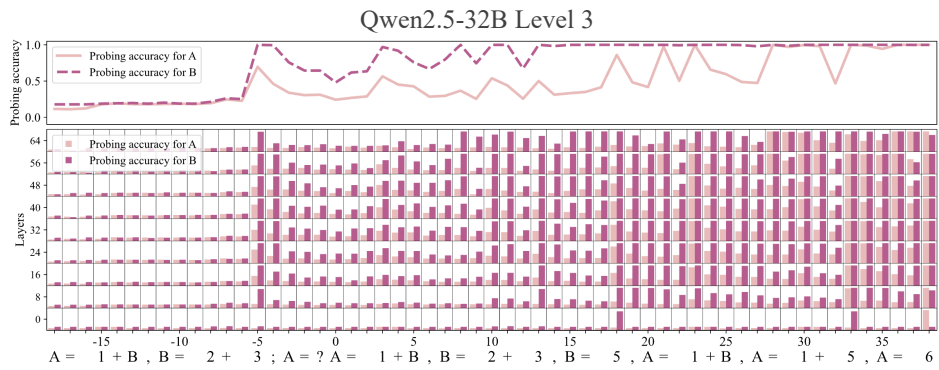


Figure 16: Probing results when Qwen2.5-32B solves Level 3.

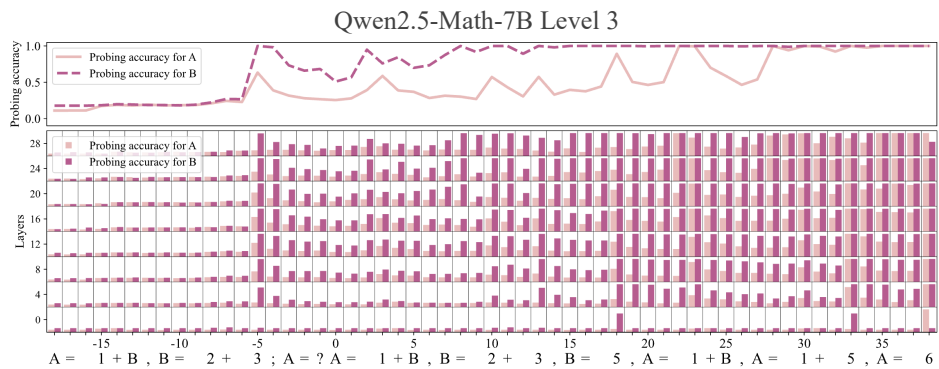


Figure 17: Probing results when Qwen2.5-Math-7B solves Level 3.

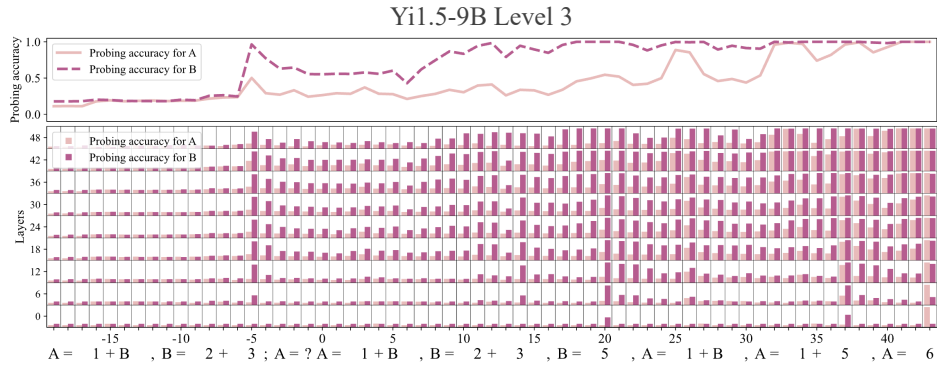


Figure 18: Probing results when Yi1.5-9B solves Level 3.

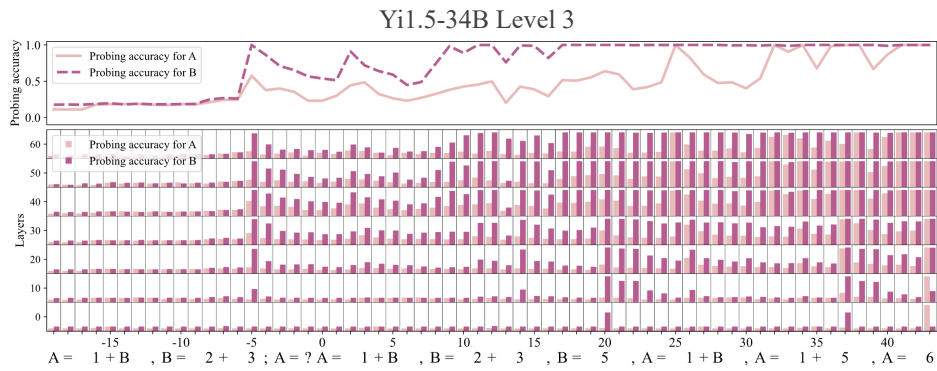


Figure 19: Probing results when Yi1.5-34B solves Level 3.

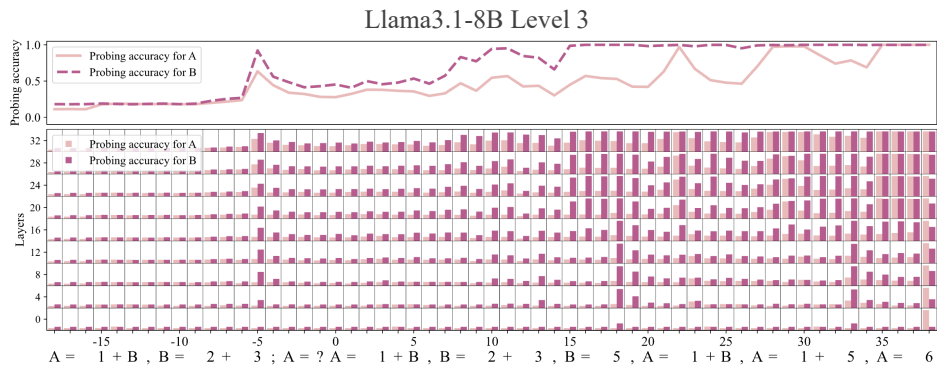


Figure 20: Probing results when Llama3.1-8B solves Level 3.

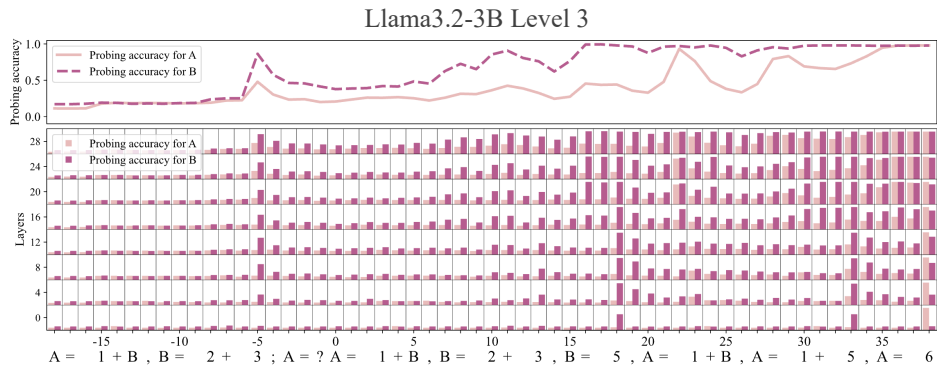


Figure 21: Probing results when Llama3.2-3B solves Level 3.

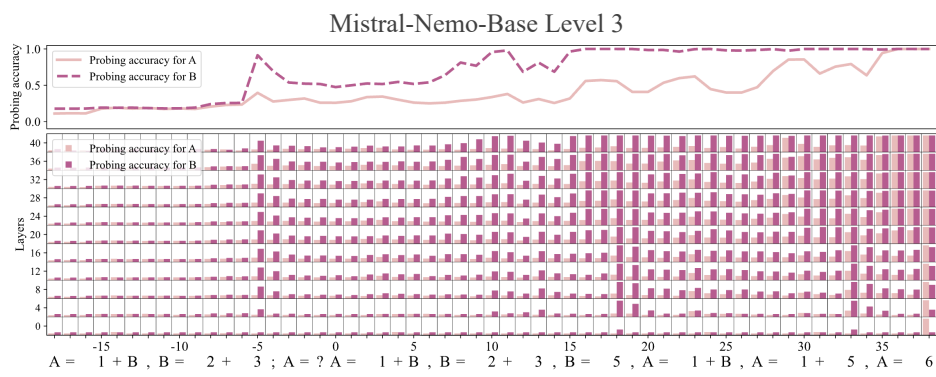


Figure 22: Probing results when Mistral-Nemo-Base solves Level 3.